# Trends in Activity and Dissolution on $RuO_2$ under Oxygen Evolution Conditions: Particles versus Well-Defined Extended Surfaces

Claudie Roy [a]; Reshma R. Rao[b]; Kelsey A. Stoerzinger [c]; Jonathan Hwang [c]; Jan Rossmeisl [d]; Ib Chorkendorff [a]; Yang Shao-Horn [b,c]; Ifan E.L. Stephens [a,e];

[a] Surface Physics and Catalysis , Department of Physics, Technical University of Denmark, DK-2800 Kgs. Lyngby, Denmark
[b] Department of Mechanical Engineering, Massachusetts Institute of Technology, Cambridge, Massachusetts 02139, United States
[c] Department of Materials Science and Engineering, Massachusetts Institute of Technology, Cambridge, Massachusetts 02139, United States
[d] Department of Chemistry, University of Copenhagen, Copenhagen, Denmark
[e] Department of Materials, Imperial College London, London, United Kingdom

**Abstract**

Rutile $RuO_2$ catalysts are the most active pure metal oxides for oxygen evolution; however, they are also unstable towards dissolution. Herein, we study the catalytic activity and stability of oriented thin films of $RuO_2$ with the (111), (101) and (001) orientations, in comparison to a (110) single crystal and commercial nanoparticles. These surfaces were all tested in aqueous solutions 0.05 M $H_2SO_4$. The initial catalyst activity ranked as follows: (001) > (101) > (111) ≈ (110). We complemented our activity data with inductively coupled plasma mass spectroscopy (ICP-MS), to measure Ru dissolution products occurring in parallel to oxygen evolution. In contrast to earlier reports, we find that, under our experimental conditions, there is no correlation between the activity and stability.

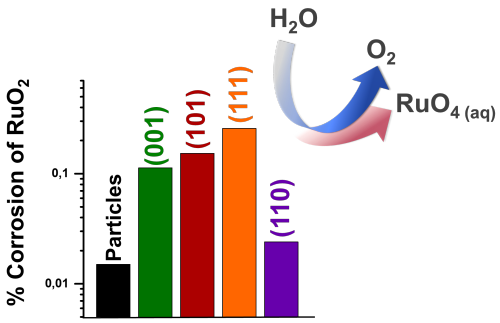
H2O
O2
RuO4 (aq)
% Corrosion of RuO2
0,1
0,01
Particles
(001)
(101)
(111)
(110)

Hydrogen production provides a means of storing electricity generated from wind and solar energy[1–3] in the form of chemical bonds. Hydrogen-based fuel cells can power vehicles and stationary devices; hydrogen could replace carbon or CO to reduce global $CO_2$ emissions from chemical and manufacturing processes. Polymer electrolyte membrane (PEM) electrolysers can synthesize hydrogen near room temperature with rapid start up and shut down,[3] ideally suited towards coupling with renewables. While hydrogen evolution, the cathode reaction occurring in a PEM electrolyzer, has minimal energy losses[4,5], the anodic reaction, i.e. oxygen evolution, is kinetically sluggish and limits the efficiency[6–8].

$$2\mathrm{H_2O} \leftrightarrow \mathrm{O_2} + 4\mathrm{H^+} + 4\mathrm{e^-} \qquad U^\circ = 1.23\,V \ \ vs\ RHE$$

The combination of an acidic environment and very positive (oxidizing) potentials sets severe constraints on the choice of catalysts for PEM electrolyser anodes[9]. Only oxides based on Ir[10,11] show reasonable activity and stability, even though they still corrode at low, yet appreciable rate[12–15]. Oxides based on Ru are more active but less stable than those based on Ir[14,16–19]. $RuO_2$ corrodes via the following reaction[20]:

$$\mathrm{RuO_2} + 2\mathrm{H_2O} \rightarrow \mathrm{RuO_4(aq)} + 4\mathrm{H^+} + 4\mathrm{e^-} \qquad U^\circ = 1.39\,V\ vs\ RHE$$

Mixed oxides of Ru and Ir exhibit a better compromise between activity and stability, forming the basis for the dimensionally stabilised anode, used extensively in the chloro-alkali industry[18,21–23].

Several reports have shown that oxygen evolution on $RuO_2$ is always associated with some degree of dissolution[14,20,24–27]. However, the Faradaic selectivity to

$RuO_2$ corrosion varies over many orders of magnitude, depending on the pretreatment: ~0.01% in the case of sputter deposited thin films in 0.05 M $H_2SO_4$[15] while it reaches values as high as ~15% for metallic Ru[11], also in 0.05 M $H_2SO_4$, and ~10% for oriented $SrRuO_3$ in 0.1 M KOH[25] (Figure 1). Figure 1 shows that $RuO_2$ obtained by thermal annealing[13,15,28–30] present, on average, 2-3 orders of magnitude lower corrosion rates than metallic Ru[11,13,20,24,29,30], perovskite oxides containing Ru[25,31], hydrated $RuO_2$[29] or plasma-treated $RuO_2$[28]. The Figure could suggest there is not a strong distinction between the rates of $RuO_x$ corrosion under acidic, relative to basic, conditions; nonetheless, we note that, Cherevko et al showed, by using identical protocols at high and low pH, that there is a slight increase in alkaline solutions[13]. This is more obvious in Figure S1 where we present the mean rate dissolution of some of the catalysts presented in Figure 1.

Over three decades ago, Kötz et al. proposed that $RuO_2$ dissolution and oxygen evolution share a common reaction pathway and the same intermediates[32]. To the best of our knowledge, most studies on Ru-based oxides, thus far, have indeed suggested a correlation between dissolution rates and activity[11,13,20,25,27,32,33]. Markovic[14] and co-workers have gone so far to argue that dissolution and oxygen evolution activity are *universally* correlated on *all* noble metal surfaces. On the other hand, Mayrhofer[27] and co-workers observed that even though the rate of dissolution increases with the onset of OER, the extent to which OER affects metal dissolution varies. Schmidt and co-workers[34] used a thermodynamic argument to explain this correlation; suggesting that $O_2$ evolution degrades the catalyst by discharging oxide anions.

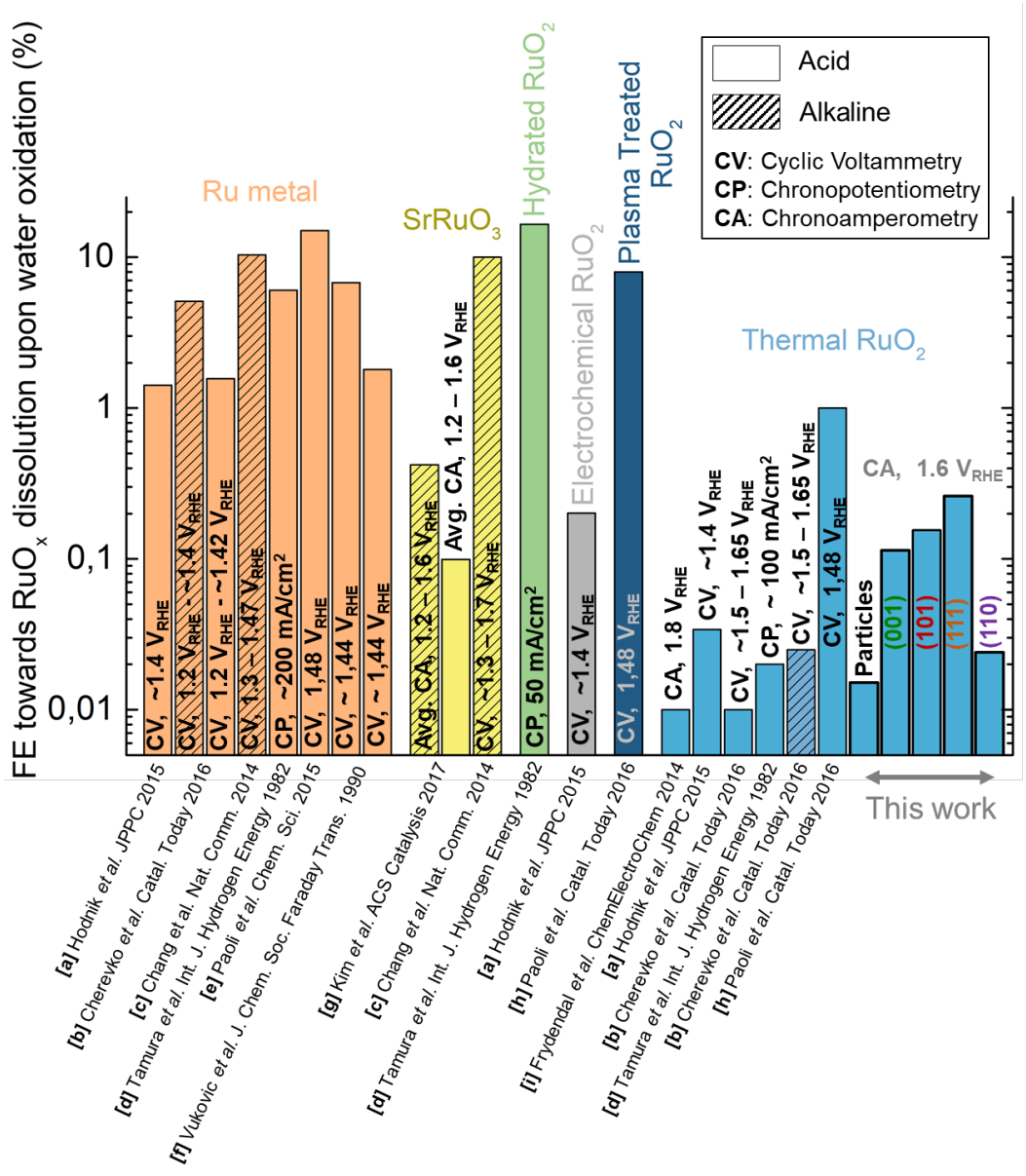


**Figure 1**. Comparison of the Faradaic efficiency of dissolution for Ru-based catalysts in acidic and alkaline electrolyte. The y axis represents the contribution of Ru dissolution to the measured current in the OER region, as a percentage. These values have been extracted from [a] Hodnik *et al*. for Ru metal,

electrochemically prepared $RuO_2$ and thermally prepared $RuO_2$. Ru dissolution measurements performed in 0.1 M $HClO_4$ using ICP-MS and at maximum of 1.4 $V_{RHE}$ [b] Cherevko *et al.* for Ru metal, and thermally prepared $RuO_2$ in 0.1 M $H_2SO_4$ and 0.05 M NaOH. Ru dissolution measured by ICP and potential scanning from 1.2 $V_{RHE}$ until reaching 5 mA/cm$^2$ [c] Chang *et al*. for polycrystalline Ru metal and oriented $SrRuO_3$ films in 0.1 M KOH. Ru dissolution measured using RRDE and scanning up to a maximum potential of ~1.485 $V_{RHE}$ for Ru and estimated to 1-10% for $SrRuO_3$. [d] Tamura *et al*. measured Ru dissolution for Ru metal at ~200 mA/cm$^2$, hydrated $RuO_2$ at ~50 mA/cm$^2$ and thermally prepared $RuO_2$ at ~100 mA/cm$^2$ in 0.5 M $H_2SO_4$ using spectrophotometric methods. [e] Paoli et al. for Ru nanoparticles in 0.05 M $H_2SO_4$ at 1.48 $V_{RHE}$ from a CV at 10 mV/s using RRDE. [f] Vukovic *et al*. electrodeposited Ru electrode. Type A electrode: as prepared electrode, Type B electrode: electrochemical activation of type A. Ru dissolution measured in 0.5 M $H_2SO_4$ using RRDE. [g] Kim *et al.* measured Ru dissolution from $SrRuO_3$ in 0.1 M KOH held at potentials from 1.2 to 1.6 $V_{RHE}$ for 60 seconds each using ICP. [h] Paoli *et al*. for Ru dissolution from plasma treated and thermally annealed $RuO_2$ nanoparticles in 0.05 M $H_2SO_4$ using RRDE [i] Frydendal *et al.* for Ru dissolution from thermally prepared sputter deposited thin films in 0.05 M $H_2SO_4$ using ICP and EQCM at a constant potential of 1.8 $V_{RHE}$. [This work] Further information can be found in Supplementary Information

Earlier DFT-based studies suggest that the reaction proceeds through a series of proton-coupled electron transfers, via the intermediates *OH, *O and *OOH (where * indicates an adsorbed species) [35,36]. The calculations suggest that $RuO_2$ has the highest activity of pure oxides because it has the most optimal compromise in binding between these different intermediates. They also indicate that the active site on the $RuO_2$ surface is a coordinately unsaturated site (CUS), located on terraces. Liu and co-workers also calculated that below 1.58$V_{NHE}$ the reaction is taking place on a OH/O mixed phase while at higher potential the reaction occurs on a fully O-terminated surface[8].

DFT simulations also suggest that undercoordinated sites, such as steps or kinks, are more likely to corrode than terrace sites, both on noble metal surfaces[37], and oxides[38,39]. Removing a terrace site requires the scission of more bonds than an undercoordinated site. Notably, recent DFT calculations by Dickens and Nørskov suggested that such undercoordinated sites are also the most catalytically active sites[40], in contrast to the aforementioned earlier studies[10,41,42].

However, our own experiments support the notion that the terrace-bound CUS sites are the active sites, as opposed to undercoordinated sites. Our in-operando surface X-ray diffraction measurements detected adsorbed *OO species on the CUS sites under oxygen evolution conditions; presumably these constitute the precursor to gas phase $O_2$ molecules[43]. Moreover, on oriented $RuO_2$ thin films in 0.1 M KOH, the oxygen evolution activity scales with the number of CUS sites on a bulk-terminated surface[44].

Summarising the above, there is significant controversy in the literature over the extent to which oxygen evolution is intrinsically related to dissolution. This question is of critical importance, as effective strategies to stabilise the catalysts require that activity and stability be decoupled from each other [18,38,39].

In the current study, we probe the oxygen evolution activity of numerous different $RuO_2$ catalysts in 0.05 M $H_2SO_4$; these include (i) thin films oriented in the (100), (001), (101), and (111) directions (previously tested in 0.1 M KOH[10,41,42]) (ii) single crystalline $RuO_2$(110)[9,44,45] and (iii) commercial $RuO_2$ particles. We only had one (110) single crystal at our disposition. We have quantified the amount of $RuO_2$

being dissolved in parallel to oxygen evolution, using inductively coupled plasma mass spectrometry (ICP-MS). In particular, we aim to address the following questions: (a) how does the OER activity compare between $RuO_2$ well-defined surfaces and particles, (b) is the corrosion of $RuO_2$ structure sensitive under oxygen evolution conditions? and (c) to what extent are activity and dissolution correlated on $RuO_2$ surfaces?

We first established the catalytic activity of the different $RuO_2$ surfaces investigated in this study, namely the (101), (111) and (001) oriented thin films and the (110) single crystal. Schematics of the bulk terminated surfaces are shown in Figure 2a. The mean value of the current density at $1.6V_{RHE}$, taken from the first CV recorded, ranks as follows: (111) thin film < (110) single crystal < particles < (101) thin film < (001) thin film (Figure S2). Comparison of the activity of the $RuO_2$ oriented thin films, single crystal and particles with other Ru-based catalysts under similar experimental conditions is available in Figure S3. In a rutile structure, Ru can form bonds with a total of 6 atoms. The $Ru_{CUS}$ at the (110) and (101) facets is linked by 5 Ru-O bonds to the rest of the structure, providing one surface site for the OER. However, the $Ru_{CUS}$ at the (001) and (111) facet forms only 4 Ru-O bonds, providing 2 empty surface sites. Consistent with our earlier reports in 0.1 M KOH[10,41,42], Figure 2b shows that the initial activity in 0.05 $MH_2SO_4$ scales with the proportion of CUS Ru-O bonds.

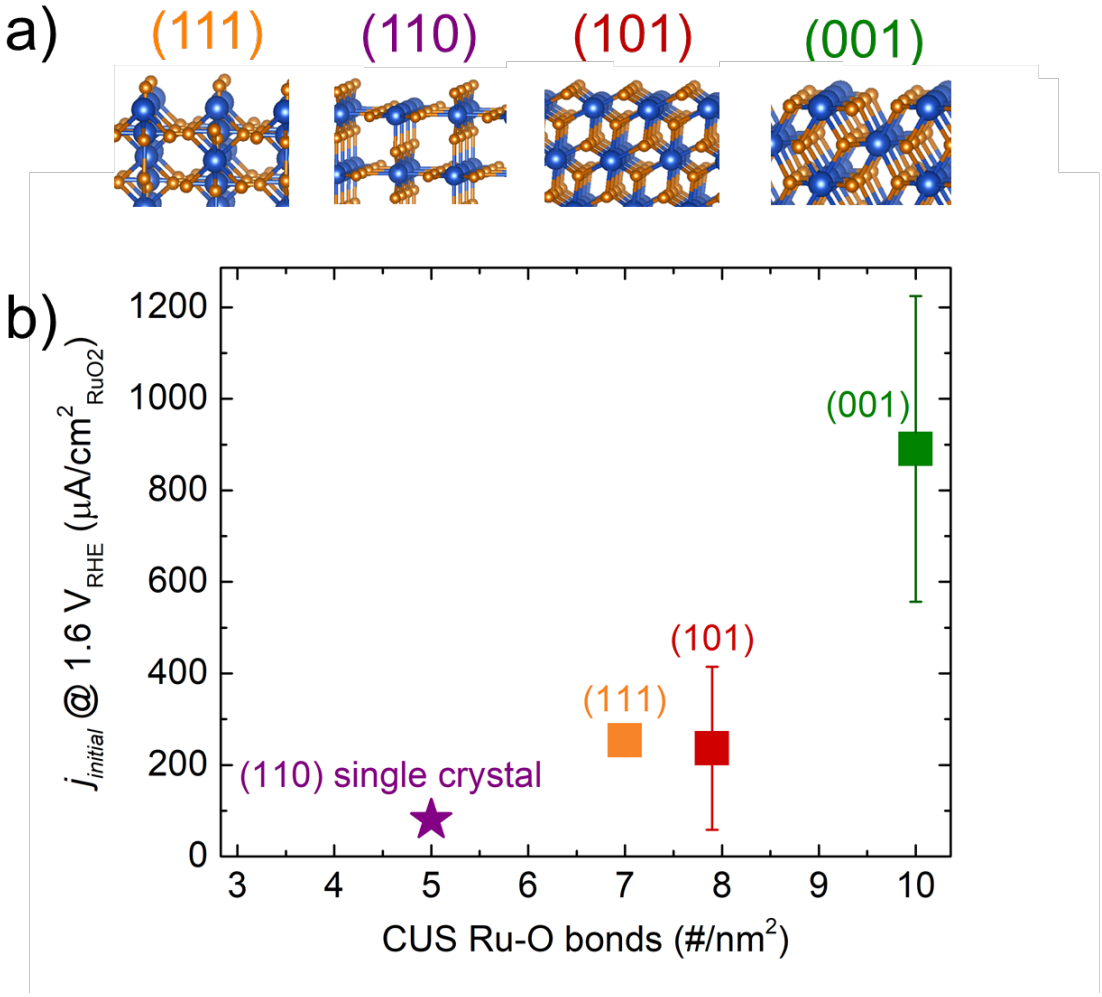


**Figure 2**. a) Schematics of the (111), (110), (101) and (001) surface and b) average current density measured the first cyclic voltammogram in 0.05 M $H_2SO_4$ over 2 hours for the (001), (111) and (101) oriented thin films and (110) single crystal, as a function of the number of CUS Ru-O bonds per $nm^2$.

Corrosion measurements on preferentially oriented thin films and $RuO_2$ particles were performed at 1.6 $V_{RHE}$ for 2h. Stability test from 1.46 to 1.7 $V_{RHE}$ using the $RuO_2$ particles and at 1.7 $V_{RHE}$ for the well-defined surfaces are also available in Figure S4-5 and Figure S6, respectively. In order to evaluate the behavior of the samples for longer periods of time, the oriented thin films that were first subjected

to the stability test at 1.6 $V_{RHE}$ were subjected to a second test, using the same experimental protocol (e.g. cycling etc, followed by the potentiostatic stability test, see Experimental). Additionally, a (110) single crystal was measured in the same experimental conditions and compared to the oriented thin films. Figure 3a and c show the OER currents measured for the first and second stability test at 1.6 $V_{RHE}$. The insets, respectively, show the amount of Ru dissolved during each experiment.

The first stability test shows a decay in the total current for the (001), (101) and (111) thin films over the 2 hours. On these films, any differences in total current densities between the different orientations is diminished by the end of the test. Conversely, the activity of the (110) single crystal at the end of the stability test is higher than the initial activity: this increase occurs during the first ~40 minutes, before reaching a steady state. The amount of Ru dissolved into the electrolyte increases in the following order: (110) single crystal < (111) thin film < (101) thin film < (001) thin film. The Faradaic efficiency towards $RuO_x$ dissolution, relative to the total current density, is less than ~0.3% for the (111) surface, ~ 0.2% for the (101) surface and ~ 0.1% for the (001) surface. The (110) single crystal and the particles have the lowest Faradaic efficiency towards corrosion, at ~ 0.02% and ~ 0.01%, respectively (Figure1). We assume that the remainder of the current is consumed by $O_2$ evolution. The detailed explanation of the Faradaic efficiency was calculated and is available in SI.

The second stability test at 1.6 $V_{RHE}$ (Figure 3c and d) reveals striking differences from the first (Figure 3a and b). In the second test, all surfaces exhibit an initial current density significantly higher than for the first test after 2h. On the other hand, the dissolution rates are much lower than the first test. For example, on the (001) film, 5 times less Ru dissolves into solution than during the first test. While the average current densities on the (001) thin film and (110) single crystal are similar, the corrosion rates are quite distinct. Moreover, the (110) single crystal shows much higher activity during the second stability test; however, its corrosion rate is similar to the first test.

Figure 3e and f show the activity show the amount of Ru dissolved as a function of activity the first and second stability test. We note that bubble build up would block both $RuO_2$ dissolution and $O_2$ in exactly the same manner. The current density shown in the initial CV (Figure S2), might be more representative of the intrinsic activity of the catalyst, as the build up of $O_2$ bubbles would not limit the current densities to the same extent. Nevertheless, we take the view that in order to probe the relationship between activity and stability towards dissolution, it is far more appropriate to correlate the Ru dissolved during the course of the potentiostatic stability test to the mean value of the current density over the same time period, as shown in Figure 3.

The variation in current density and Ru dissolution rate for the different crystallographic surfaces show that both activity and stability are surface specific. In the first test at 1.6 $V_{RHE}$, there is a positive correlation between activity and dissolution rates amongst the thin film samples. However, the particles and the

single crystal show much lower values for the average activity than the films, and intermediate dissolution rates. The (110) single crystal and the $RuO_2$ particles have very similar average catalytic activity during the first stability test, at around 45 $\mu A/cm^2$.This observation is consistent with the transmission electron microscopy and X-ray diffraction analyses, which suggest the nanoparticles have a preferential orientation along the (110) planes (see Figure S7).

The second stability test reveals a totally different trend. While in the first test, there was a clear correlation between activity and stability amongst the thin films, there was no such correlation in the second test. The $RuO_2$ (110) single crystal surface showed the highest activity and stability (lowest amount of dissolved Ru). The activity of the oriented thin films decrease slightly during the second test, while the amount of Ru dissolved is significantly lower. The activity of the $RuO_2$ particles decreases too but the Ru dissolution stays similar. The activity of the (110) single crystal increased while the total Ru dissolution decreased. Figure S8 compares of the Ru dissolution rate to the activity recorded by cyclic voltammetry before and after stability tests.

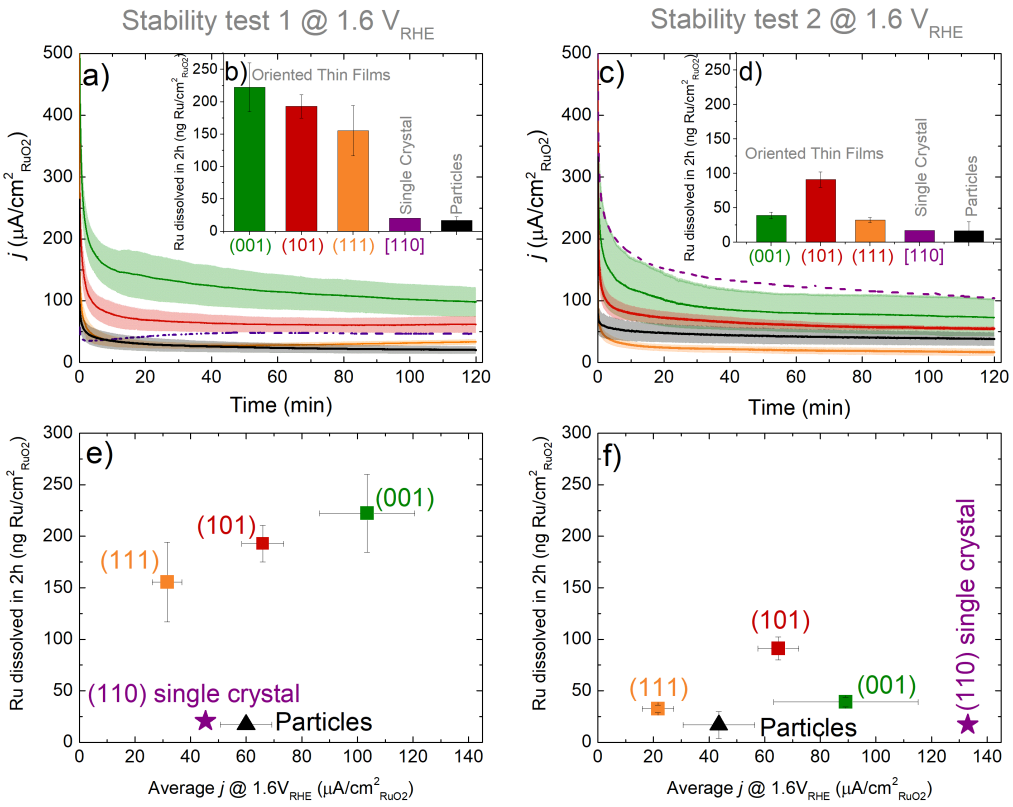


**Figure 3**. Two-hour potentiostatic measurements at 1.6 $V_{RHE}$ in 0.05 M $H_2SO_4$ a) First stability and c) second stability test for the $RuO_2$ particles, and (111), (101), (110) and (001) surfaces. The insets (b,d) show the amount of Ru dissolved for each sample measured for their respective stability test. e) and f) Evaluation of the activity-stability relationship through the analysis of the average current at 1.6 $V_{RHE}$ obtained from the stability tests as function of the amount of Ru dissolved for e) the first and f) second stability test at 1.6 $V_{RHE}$, respectively. The squares represented the (001), (101), (111) oriented thin films, the start the (110) single crystal and triangles the commercial $RuO_2$ particles.

The fact that we always observe some degree of corrosion of $RuO_2$ particles and the well-defined thin films (Figure 3) is consistent with earlier reports in the literature[13,14,20,25]. On average, the current corresponding to Ru dissolution is $\leq 0.3\%$ of the total OER current; we thus approximate the oxygen evolution current density to be equal to the total current density. This low Faradaic selectivity to corrosion is comparable to the values obtained from heat treated $RuO_2$ nanoparticles[28] or sputter deposited $RuO_2$[15] under similar experimental conditions. The dissolution of $RuO_2$ translates into an increase in surface roughness, corroborated by the enhanced capacitance value, following the stability test (Figure S9-11). We calculate that the amount of Ru dissolved at 1.6 $V_{RHE}$ over the duration of the 2 hour stability test ranges between 1.5 to 2.5 ML, depending on the surface orientation. Consequently, by the end of the first stability test, the surface termination may differ appreciably from the pristine surface. However, while Ru dissolution most probably modifies the surface termination, it only represents up to ~4% of the total amount of Ru in the 25 nm thin film.

In this work, we also note that the potentiostatic measurements suggest a loss in catalytic activity over time, implying that the freshly exposed surface, formed a result of dissolution has a distinct $RuO_2$ termination to the as-prepared surface (Figures S6-8).

The decrease in activity during the chronoamperometry measurements can also be related to bubble formation. The static electrode configuration increases the amount of bubbles at the surface of the catalysts, blocking more active sites than when using a rotating disk electrode setup. This phenomenon is evident when

comparing the current density at the end of the 2 hours of the first stability test 1.6 V (Figure S12), relative to the current density at the beginning of the second stability test (Figure S12); bubbles were removed between tests. In this case, it turns out that the hydrophobicity of the $RuO_2$ surfaces does not play a determining role in the activity measurement, i.e. the activity measured by CV is comparable to the average current by CA, as shown in Figure S13.

We consider that our measurements underestimate the intrinsic dissolution rates of $RuO_2$ particles: the addition of Nafion to the ink preparation may result in lower mobility and higher local concentrations of Ru cations in solution, stabilising the surface. Moreover, it is worth mentioning that we observed some degree of degradation of the substrate when using FTO, which could partially explain the loss in activity over time [46].

Using the Ru dissolution rates and the current measured at constant potential, we aimed to establish a relationship between the oxygen evolution activity of $RuO_2$ and its stability. However, our finding contrasts strongly with other reports of Ru-based catalysts both tested in alkaline[13,25] and acid[13,14,41,47], which show a consistent correlation between Ru dissolution rates and activity. The currents and $RuO_2$ dissolution rates from the first potentiostatic measurements at 1.6 $V_{RHE}$ (Figure 3) decrease in the order (001) > (101) > (111). However, for the second test, there is no correlation between activity and stability. We speculate that the drastic increase in current density of the $RuO_2$ (110) single crystal could be due to surface reconstruction. Our observations show that the corrosion rates are intrinsically dependent on the surface structure. When comparing the first stability

test at 1.6$V_{RHE}$ to the second one (Figure 3), it seems that the sites responsible from the OER activity and stability are decoupled; the change in $RuO_2$ dissolution rates between first and second stability tests are not matched by changes in activity. During the first stability test, the (001) surface has the most active and most unstable surface: the lower corrosion rate, but similar oxygen evolution activity, during the second test, suggests that the sites most prone to corrosion have dissolved away, while the active sites for $O_2$ evolution remain.

Our results support the notion that the density of surface defects, such as undercoordinated sites, play a major role in controlling the stability of surface atoms[3,13,37–39]. We suggest that (001) thin films contain the highest initial amount of surface defects, followed by the (101), (111) and (110). We hypothesize that the amount of defects on the as-received particles and single crystal is significantly lower than on the oriented thin film, explaining the much lower corrosion rate during the first corrosion test. In a similar manner, the $RuO_2$ particles and (110) single crystal have a similar initial activity but different initial corrosion rates. Our results show that $RuO_x$ corrosion is generally much more pronounced during the first stability test. We conjecture that the amount of defects decreases over time before reaching a more stable state. Indeed, during the second stability test, with the exception of the (101) surface, there is little difference between the corrosion rates of the various surfaces.

The aim of this work was to investigate the possible relationship between activity and stability obtained from $RuO_2$ particles, preferentially oriented $RuO_2$ surfaces and a single crystal. The correlation between the activity and CUS Ru-O bonds reported in this study corroborates the previous results in base[41]. We therefore propose that the active site for oxygen evolution in 0.05 M $H_2SO_4$ to be the $Ru_{CUS}$ site.

We performed potentiostatic measurements of $RuO_2$ electrodes, coupled with ICP-MS to probe $RuO_2$ dissolution. On the basis of our results, we propose that surface structure not only has an important role in controlling activity, but also corrosion. From the first stability test at 1.6 $V_{RHE}$, it appears that corrosion of $RuO_2$ is structure sensitive. However, the active sites responsible for the oxygen evolution seem to be decoupled from the Ru sites that corrode the fastest. *In other words, activity and stability do not appear to be correlated on $RuO_2$ surfaces*. Based on the assumption that undercoordinated sites are responsible for dissolution, we conjecture that they are not the active sites for oxygen evolution under our experimental conditions. More detailed investigations of the surface structure are needed to elucidate the changes induced by the electrochemical environment[44,48,49].

The evidence we provide herein, suggesting that oxygen evolution and dissolution occur from different sites, has profound implications on future catalyst design. Such understanding corroborates our earlier work on the role of surface Ir in stabilising $RuO_x$[18] and surface Ti on MnOx[39], without compromising activity. Such

work points to ample opportunities for engendering further improvements to the stability of oxygen evolution catalysts under acidic conditions.

**Supporting information**
The Supporting Information is available free of charge on the ACS Publications website at DOI: XXXXX

A description of the experimental methods, additional characterization, electrochemical testing, and microscopy images included in the SI

## Author Information and notes

## Acknowledgements

We thank Binghong Han for TEM characterization of $RuO_2$ nanoparticles. We also thank Hoydoo You from the Argonne National Laboratory for providing us the (110) single crystal. C.R. gratefully acknowledges the Ministry of Higher Education and Science and Otto Mønsteds Fond for awarding her the visiting researcher grant. I.E.L.S. gratefully acknowledges the Department of Mechanical Engineering at MIT for the Peabody Visiting Associate Professorship. This work was supported by a research grant (9455) from VILLUM FONDEN. We also acknowledge UPCAT under the project no. 2015-1-12315 from energinet.dk. The film growth and structural characterization at ORNL were supported by the U.S. Department of Energy, Office of Science, Basic Energy Sciences, Materials Sciences and Engineering Division. This work is supported in part by the Skoltech-MIT Center for Electrochemical Energy and the Cooperative Agreement between the Masdar Institute, Abu Dhabi, UAE, and MIT (02/MI/MIT/CP/11/07633/GEN/G/ 00).

(1) Montoya, J. H.; Seitz, L. C.; Chakthranont, P.; Vojvodic, A.; Jaramillo, T. F.; Nørskov, J. K. Materials for Solar Fuels and Chemicals. *Nat. Mater.* **2017**, *16* (1), 70–81 DOI: 10.1038/nmat4778.

(2) Carmo, M.; Fritz, D. L.; Mergel, J.; Stolten, D. A Comprehensive Review on PEM Water Electrolysis. *Int. J. Hydrogen Energy* **2013**, *38* (12), 4901–4934 DOI: 10.1016/j.ijhydene.2013.01.151.

(3) Stamenkovic, V. R.; Strmcnik, D.; Lopes, P. P.; Markovic, N. M. Energy and Fuels from Electrochemical Interfaces. *Nat. Mater.* **2017**, *16* (1), 57–69 DOI: 10.1038/nmat4738.

(4) Durst, J.; Siebel, A.; Simon, C.; Hasché, F.; Herranz, J.; Gasteiger, H. A. New Insights into the Electrochemical Hydrogen Oxidation and Evolution Reaction Mechanism. *Energy Environ. Sci.* **2014**, *7* (7), 2255–2260 DOI: 10.1039/C4EE00440J.

(5) Zalitis, C. M.; Sharman, J.; Wright, E.; Kucernak, A. R. Properties of the Hydrogen Oxidation Reaction on Pt/C Catalysts at Optimised High Mass Transport Conditions and its Relevance to the Anode Reaction in PEFCs and Cathode Reactions in Electrolysers. *Electrochim. Acta* **2015**, *176*, 763–776 DOI: 10.1016/j.electacta.2015.06.146.

(6) Hong, W. T.; Risch, M.; Stoerzinger, K. A.; Grimaud, A.; Suntivich, J.; Shao-Horn, Y. Toward the Rational Design of Non-Precious Transition Metal Oxides for Oxygen Electrocatalysis. *Energy Environ. Sci.* **2015**, *8* (5), 1404–1427 DOI: 10.1039/C4EE03869J.

(7) Seh, Z. W.; Kibsgaard, J.; Dickens, C. F.; Chorkendorff, I.; Nørskov, J. K.; Jaramillo, T. F. Combining Theory and Experiment in Electrocatalysis: Insights into Materials Design. *Science (80-. ).* **2017**, *355* (6321), eaad4998 DOI: 10.1126/science.aad4998.

(8) Fang, Y.-H.; Liu, Z.-P. Mechanism and Tafel Lines of Electro-Oxidation of Water to Oxygen on $RuO_2$ (110). *J. Am. Chem. Soc.* **2010**, *132* (51), 18214–18222 DOI: 10.1021/ja1069272.

(9) Castelli, P.; Trasatti, S.; Pollak, F. H.; O'Grady, W. E. Single Crystals as Model Electrocatalysts. *J. Electroanal. Chem. Interfacial Electrochem.* **1986**, *210* (1), 189–194 DOI: 10.1016/0022-0728(86)90325-6.

(10) Stoerzinger, K. A.; Qiao, L.; Biegalski, M. D.; Shao-Horn, Y. Orientation-Dependent Oxygen Evolution Activities of Rutile $IrO_2$ and $RuO_2$. *J. Phys. Chem. Lett.* **2014**, *5* (10), 1636–1641 DOI: 10.1021/jz500610u.

(11) Paoli, E. A.; Masini, F.; Frydendal, R.; Deiana, D.; Schlaup, C.; Malizia, M.; Hansen, T. W.; Horch, S.; Stephens, I. E. L.; Chorkendorff, I. Oxygen Evolution on Well-Characterized Mass-Selected Ru and $RuO_2$ Nanoparticles. *Chem. Sci.* **2015**, *6* (1), 190–196 DOI: 10.1039/C4SC02685C.

(12) Kasian, O.; Grote, J.-P.; Geiger, S.; Cherevko, S.; Mayrhofer, K. J. J. The Common Intermediates of Oxygen Evolution and Dissolution Reactions during Water Electrolysis on Iridium. *Angew. Chemie Int. Ed.* **2018**, *57* (9), 2488–2491 DOI: 10.1002/anie.201709652.

(13) Cherevko, S.; Geiger, S.; Kasian, O.; Kulyk, N.; Grote, J.-P.; Savan, A.; Shrestha, B. R.; Merzlikin, S.; Breitbach, B.; Ludwig, A.; et al. Oxygen and Hydrogen Evolution Reactions on Ru, $RuO_2$ , Ir, and $IrO_2$ Thin Film Electrodes in Acidic and Alkaline Electrolytes: A Comparative Study on Activity and Stability. *Catal. Today* **2016**, *262*, 170–180 DOI: 10.1016/j.cattod.2015.08.014.

(14) Danilovic, N.; Subbaraman, R.; Chang, K.-C.; Chang, S. H.; Kang, Y. J.; Snyder, J.; Paulikas, A. P.; Strmcnik, D.; Kim, Y.-T.; Myers, D.; et al. Activity–Stability Trends for the Oxygen Evolution Reaction on Monometallic Oxides in Acidic Environments. *J. Phys. Chem. Lett.* **2014**, *5* (14), 2474–2478 DOI: 10.1021/jz501061n.

(15) Frydendal, R.; Paoli, E. A.; Knudsen, B. P.; Wickman, B.; Malacrida, P.; Stephens, I. E. L.; Chorkendorff, I. Benchmarking the Stability of Oxygen Evolution Reaction Catalysts: The Importance of Monitoring Mass Losses. *ChemElectroChem* **2014**, *1* (12), 2075–2081 DOI: 10.1002/celc.201402262.

(16) Kötz, R.; Stucki, S. Stabilization of $RuO_2$ by $IrO_2$ for Anodic Oxygen Evolution in Acid Media. *Electrochem. Acta* **1986**, *31* (10), 1311–1316.

(17) Cherevko, S.; Reier, T.; Zeradjanin, A. R.; Pawolek, Z.; Strasser, P.; Mayrhofer, K. J. J. Stability of Nanostructured Iridium Oxide Electrocatalysts During Oxygen Evolution Reaction in Acidic Environment. *Electrochem. commun.* **2014**, *48*, 81–85 DOI:

10.1016/j.elecom.2014.08.027.

(18) Escudero-Escribano, M.; Pedersen, A. F.; Paoli, E. A.; Frydendal, R.; Friebel, D.; Malacrida, P.; Rossmeisl, J.; Stephens, I. E. L.; Chorkendorff, I. Importance of Surface $IrO_x$ in Stabilizing $RuO_2$ for Oxygen Evolution. *J. Phys. Chem. B* **2018**, *122* (2), 947–955 DOI: 10.1021/acs.jpcb.7b07047.

(19) Danilovic, N.; Subbaraman, R.; Chang, K. C.; Chang, S. H.; Kang, Y.; Snyder, J.; Paulikas, A. P.; Strmcnik, D.; Kim, Y. T.; Myers, D.; et al. Using Surface Segregation To Design Stable Ru-Ir Oxides for the Oxygen Evolution Reaction in Acidic Environments. *Angew. Chemie Int. Ed.* **2014**, *53* (51), 14016–14021 DOI: 10.1002/anie.201406455.

(20) Vuković, M. Rotating Ring–Disc Electrode Study of the Enhanced Oxygen Evolution on an Activated Ruthenium Electrode. *J. Chem. Soc., Faraday Trans.* **1990**, *86* (22), 3743–3746 DOI: 10.1039/FT9908603743.

(21) Beer, H. B. The Invention and Industrial Development of Metal Anodes. *J. Electrochem. Soc.* **1980**, *127* (8), 303C–307C DOI: 10.1149/1.2130021.

(22) Trasatti, S. Electrocatalysis: Understanding the Success of DSA®. *Electrochim. Acta* **2000**, *45* (15–16), 2377–2385 DOI: 10.1016/S0013-4686(00)00338-8.

(23) Kasian, O.; Geiger, S.; Stock, P.; Polymeros, G.; Breitbach, B.; Savan, A.; Ludwig, A.; Cherevko, S.; Mayrhofer, K. J. J. On the Origin of the Improved Ruthenium Stability in $RuO_2$ –$IrO_2$ Mixed Oxides. *J. Electrochem. Soc.*

**2016**, *163* (11), F3099–F3104 DOI: 10.1149/2.0131611jes.

(24) Chang, S. H.; Connell, J. G.; Danilovic, N.; Subbaraman, R.; Chang, K.-C.; Stamenkovic, V. R.; Markovic, N. M. Activity–Stability Relationship in the Surface Electrochemistry of the Oxygen Evolution Reaction. *Faraday Discuss.* **2014**, *176* (0), 125–133 DOI: 10.1039/C4FD00134F.

(25) Chang, S. H.; Danilovic, N.; Chang, K.-C.; Subbaraman, R.; Paulikas, A. P.; Fong, D. D.; Highland, M. J.; Baldo, P. M.; Stamenkovic, V. R.; Freeland, J. W.; et al. Functional Links between Stability and Reactivity of Strontium Ruthenate Single Crystals during Oxygen Evolution. *Nat. Commun.* **2014**, *5* (1), 4191 DOI: 10.1038/ncomms5191.

(26) Lopes, P. P.; Strmcnik, D.; Tripkovic, D.; Connell, J. G.; Stamenkovic, V.; Markovic, N. M. Relationships between Atomic Level Surface Structure and Stability/Activity of Platinum Surface Atoms in Aqueous Environments. *ACS Catal.* **2016**, *6* (4), 2536–2544 DOI: 10.1021/acscatal.5b02920.

(27) Cherevko, S.; Zeradjanin, A. R.; Topalov, A. a.; Kulyk, N.; Katsounaros, I.; Mayrhofer, K. J. J. Dissolution of Noble Metals during Oxygen Evolution in Acidic Media. *ChemCatChem* **2014**, *6* (8), 2219–2223 DOI: 10.1002/cctc.201402194.

(28) Paoli, E. A.; Masini, F.; Frydendal, R.; Deiana, D.; Malacrida, P.; Hansen, T. W.; Chorkendorff, I.; Stephens, I. E. L. Fine-tuning the Activity of Oxygen Evolution Catalysts: The Effect of Oxidation Pre-Treatment on Size-Selected Ru Nanoparticles. *Catal. Today* **2016**, *262*, 57–64 DOI:

10.1016/j.cattod.2015.10.005.

(29) Tamura, H.; Iwakura, C. Metal Oxide Anodes for Oxygen Evolution. *Int. J. Hydrogen Energy* **1982**, *7* (11), 857–865 DOI: 10.1016/0360-3199(82)90003-9.

(30) Hodnik, N.; Jovanovič, P.; Pavlišič, A.; Jozinović, B.; Zorko, M.; Bele, M.; Šelih, V. S.; Šala, M.; Hočevar, S.; Gaberščček, M. New Insights into Corrosion of Ruthenium and Ruthenium Oxide Nanoparticles in Acidic Media. *J. Phys. Chem. C* **2015**, *119* (18), 10140–10147 DOI: 10.1021/acs.jpcc.5b01832.

(31) Kim, B.-J.; Abbott, D. F.; Cheng, X.; Fabbri, E.; Nachtegaal, M.; Bozza, F.; Castelli, I. E.; Lebedev, D.; Schäublin, R.; Copéret, C.; et al. Unraveling Thermodynamics, Stability, and Oxygen Evolution Activity of Strontium Ruthenium Perovskite Oxide. *ACS Catal.* **2017**, *7* (5), 3245–3256 DOI: 10.1021/acscatal.6b03171.

(32) Kötz, R.; Stucki, S.; Scherson, D.; Kolb, D. M. In-situ Identification of $RuO_4$ as the Corrosion Product during Oxygen Evolution on Ruthenium in Acid Media. *J. Electroanal. Chem.* **1984**, *172* (1–2), 211–219 DOI: 10.1016/0022-0728(84)80187-4.

(33) Reier, T.; Nong, H. N.; Teschner, D.; Schlögl, R.; Strasser, P. Electrocatalytic Oxygen Evolution Reaction in Acidic Environments - Reaction Mechanisms and Catalysts. *Adv. Energy Mater.* **2017**, *7* (1), 1601275 DOI: 10.1002/aenm.201601275.

(34) Binninger, T.; Mohamed, R.; Waltar, K.; Fabbri, E.; Levecque, P.; Kötz, R.; Schmidt, T. J. Thermodynamic Explanation of the Universal Correlation between Oxygen Evolution Activity and Corrosion of Oxide Catalysts. *Sci. Rep.* **2015**, *5* (1), 12167 DOI: 10.1038/srep12167.

(35) Rossmeisl, J.; Qu, Z.-W.; Zhu, H.; Kroes, G.-J.; Nørskov, J. K. Electrolysis of Water on Oxide Surfaces. *J. Electroanal. Chem.* **2007**, *607* (1–2), 83–89 DOI: 10.1016/j.jelechem.2006.11.008.

(36) Man, I. C.; Su, H.-Y.; Calle-Vallejo, F.; Hansen, H. A.; Martínez, J. I.; Inoglu, N. G.; Kitchin, J.; Jaramillo, T. F.; Nørskov, J. K.; Rossmeisl, J. Universality in Oxygen Evolution Electrocatalysis on Oxide Surfaces. *ChemCatChem* **2011**, *3* (7), 1159–1165 DOI: 10.1002/cctc.201000397.

(37) Jinnouchi, R.; Toyoda, E.; Hatanaka, T.; Morimoto, Y. First Principles Calculations on Site-Dependent Dissolution Potentials of Supported and Unsupported Pt Particles. *J. Phys. Chem. C* **2010**, *114* (41), 17557–17568 DOI: 10.1021/jp106593d.

(38) Man, I. Theorectical study of Photo-Catalytic oxygen evolution, Technical University of Denmark, 2011.

(39) Frydendal, R.; Paoli, E. A.; Chorkendorff, I.; Rossmeisl, J.; Stephens, I. E. L. Toward an Active and Stable Catalyst for Oxygen Evolution in Acidic Media: Ti-Stabilized $MnO_2$. *Adv. Energy Mater.* **2015**, *5* (22), 1500991 DOI: 10.1002/aenm.201500991.

(40) Dickens, C. F.; Nørskov, J. K. A Theoretical Investigation into the Role of Surface Defects for Oxygen Evolution on $RuO_2$. *J. Phys. Chem. C* **2017**, *121* (34), 18516–18524 DOI: 10.1021/acs.jpcc.7b03481.

(41) Stoerzinger, K. A.; Diaz-Morales, O.; Kolb, M.; Rao, R. R.; Frydendal, R.; Qiao, L.; Wang, X. R.; Halck, N. B.; Rossmeisl, J.; Hansen, H. A.; et al. Orientation-Dependent Oxygen Evolution on $RuO_2$ without Lattice Exchange. *ACS Energy Lett.* **2017**, *2* (4), 876–881 DOI: 10.1021/acsenergylett.7b00135.

(42) Stoerzinger, K. A.; Rao, R. R.; Wang, X. R.; Hong, W. T.; Rouleau, C. M.; Shao-Horn, Y. The Role of Ru Redox in pH-Dependent Oxygen Evolution on Rutile Ruthenium Dioxide Surfaces. *Chem* **2017**, *2* (5), 668–675 DOI: 10.1016/j.chempr.2017.04.001.

(43) Pedersen, A. F.; Escudero-Escribano, M.; Sebok, B.; Bodin, A.; Paoli, E.; Frydendal, R.; Friebel, D.; Stephens, I. E. L.; Rossmeisl, J.; Chorkendorff, I.; et al. Operando XAS Study of the Surface Oxidation State on a Monolayer $IrO_x$ on $RuO_x$ and Ru Oxide Based Nanoparticles for Oxygen Evolution in Acidic Media. *J. Phys. Chem. B* **2018**, *122* (2), 878–887 DOI: 10.1021/acs.jpcb.7b06982.

(44) Rao, R. R.; Kolb, M. J.; Halck, N. B.; Pedersen, A. F.; Mehta, A.; You, H.; Stoerzinger, K. A.; Feng, Z.; Hansen, H. A.; Zhou, H.; et al. Towards Identifying the Active Sites on $RuO_2$ (110) in Catalyzing Oxygen Evolution. *Energy Environ. Sci.* **2017**, *10* (12), 2626–2637 DOI:

10.1039/C7EE02307C.

(45) Lister, T. .; Chu, Y.; Cullen, W.; You, H.; Yonco, R. .; Mitchell, J. .; Nagy, Z. Electrochemical and X-ray Scattering Study of Well Defined $RuO_2$ Single Crystal Surfaces. *J. Electroanal. Chem.* **2002**, *524–525*, 201–218 DOI: 10.1016/S0022-0728(02)00744-1.

(46) Geiger, S.; Kasian, O.; Mingers, A. M.; Nicley, S. S.; Haenen, K.; Mayrhofer, K. J. J.; Cherevko, S. Catalyst Stability Benchmarking for the Oxygen Evolution Reaction: The Importance of Backing Electrode Material and Dissolution in Accelerated Aging Studies. *ChemSusChem* **2017**, *10* (21), 4140–4143 DOI: 10.1002/cssc.201701523.

(47) Frydendal, R.; Busch, M.; Halck, N. B.; Paoli, E. A.; Krtil, P.; Chorkendorff, I.; Rossmeisl, J. Enhancing Activity for the Oxygen Evolution Reaction: The Beneficial Interaction of Gold with Manganese and Cobalt Oxides. *ChemCatChem* **2015**, *7* (1), 149–154 DOI: 10.1002/cctc.201402756.

(48) Hussain, H.; Tocci, G.; Woolcot, T.; Torrelles, X.; Pang, C. L.; Humphrey, D. S.; Yim, C. M.; Grinter, D. C.; Cabailh, G.; Bikondoa, O.; et al. Structure of a Model $TiO_2$ Photocatalytic Interface. *Nat. Mater.* **2017**, *16* (4), 461–466 DOI: 10.1038/nmat4793.

(49) Li, T.; Kasian, O.; Cherevko, S.; Zhang, S.; Geiger, S.; Scheu, C.; Felfer, P.; Raabe, D.; Gault, B.; Mayrhofer, K. J. J. Atomic-Scale Insights into Surface Species of Electrocatalysts in Three Dimensions. *Nat. Catal.* **2018**, *1* (4), 300–305 DOI: 10.1038/s41929-018-0043-3.

(50) Lister, T. E.; Tolmachev, Y. V.; Chu, Y.; Cullen, W. G.; You, H.; Yonco, R.; Nagy, Z. Cathodic Activation of RuO2 Single Crystal Surfaces for Hydrogen-Evolution Reaction. *J. Electroanal. Chem.* **2003**, *554–555* (1), 71–76 DOI: 10.1016/S0022-0728(03)00048-2.